The Astrophysical Journal Letters, 974:L16 (9pp), 2024 October 10 https://doi.org/10.3847/2041-8213/ad7bbc
© 2024. The Author(s). Published by the American Astronomical Society.
OPEN ACCESS

Mitigating the Binary Viewing Angle Bias for Standard Sirens

Alberto Salvarese and Hsin-Yu Chen
Department of Physics, The University of Texas at Austin, 2515 Speedway, Austin, TX 78712, USA; alberto.salvarese@utexas.edu
Received 2024 June 27; revised 2024 September 9; accepted 2024 September 16; published 2024 October 9

Abstract

The inconsistency between experiments in the measurements of the local Universe expansion rate, the Hubble constant, suggests unknown systematics in the existing experiments or new physics. Gravitational-wave standard sirens, a method to independently provide direct measurements of the Hubble constant, have the potential to address this tension. Before that, it is critical to ensure there are no substantial systematics in the standard siren method. A significant systematic has been identified when the viewing angle of the gravitational-wave sources, the compact binary coalescences, was inferred inaccurately from electromagnetic observations of the sources. Such a systematic has led to a more than 10% discrepancy in the standard siren Hubble constant measurements with the observations of binary neutron star merger, GW170817. In this Letter, we develop a new formalism to infer and mitigate this systematic. We demonstrate that the systematic uncertainty of the Hubble constant measurements can be reduced to a level smaller than their statistical uncertainty with 5, 10, and 20 binary neutron star merger observations. We show that our formalism successfully reduces the systematics even if the shape of the biased viewing angle distribution does not follow precisely the model we choose. Our formalism ensures unbiased standard siren Hubble constant measurements when the binary viewing angles are inferred from electromagnetic observations.

Unified Astronomy Thesaurus concepts: Cosmological parameters (339); Gravitational waves (678); Neutron stars (1108)

1. Introduction

The expansion rate of the local Universe, the Hubble constant (H_0), is one of the most important constants in modern cosmology. Despite numerous observational efforts, a statistically significant discrepancy persists between direct measurements and indirect inferences of H_0 (A. J. Ross et al. 2015; A. G. Riess et al. 2016; S. Alam et al. 2017; L. Verde et al. 2019; N. Aghanim et al. 2020; E. Di Valentino et al. 2021; M. Kamionkowski & A. G. Riess 2023). For example, the tension between the Hubble constant measured by the SH0ES team using Type Ia supernovae ($H_0 = 73.3 \pm 1.04\,\mathrm{km\,s^{-1}\,Mpc^{-1}}$; A. G. Riess et al. 2022) and inferred by Planck collaboration using the cosmic microwave background ($H_0 = 67.4 \pm 0.5\,\mathrm{km\,s^{-1}\,Mpc^{-1}}$; N. Aghanim et al. 2020) is as large as ∼8%.

Gravitational-wave (GW) observations of compact binary coalescences (CBCs) offer an independent and direct measurement of H_0. The luminosity distance to CBCs can be inferred from the amplitude of the GW signals. When combining with the redshift estimates, we can measure the cosmological parameters (B. F. Schutz 1986). This is known as the "standard siren" method. Nearby CBCs ($z \lesssim 0.1$) are ideal for the measurement of H_0. There are several possibilities to estimate the redshift of CBCs. If an electromagnetic (EM) counterpart of a CBC is observed, it is possible to precisely localize the CBC's host galaxy and determine the redshift from spectral follow-up or existing galaxy catalogs (B. F. Schutz 1986; D. E. Holz & S. A. Hughes 2005). With about 50 CBCs and their EM counterparts, H_0 can be determined to ∼2% precision, shedding light on the Hubble tension (B. F. Schutz 1986; S. Nissanke et al. 2013; H.-Y. Chen et al. 2018; S. M. Feeney et al. 2019).

Furthermore, it is known that the precision of standard siren measurements can be improved by constraining the CBC's viewing angle (ι) (P. A. Evans et al. 2017; R. Margutti et al. 2017; D. Finstad et al. 2018; K. P. Mooley et al. 2018; Y. Wu & A. MacFadyen 2018; H.-Y. Chen et al. 2019). GW emissions from a CBC are anisotropic. The emissions are stronger along the rotational axis of binaries. Therefore, signals received from a faraway face-on binary are similar to those from a nearby edge-on binary (B. P. Abbott et al. 2019). By constraining the viewing angle, the degeneracy between binary distance and viewing angle can be broken, tightening the estimate of luminosity distance and reducing the uncertainty of H_0 measurements (H.-Y. Chen et al. 2019). Nicely, the observations of EM counterparts not only provide the redshift estimate but also allow for the measurement of a CBC's viewing angle. The observations of the jet and afterglow of gamma-ray burst and kilonova following the binary neutron star (BNS) merger, GW170817 (B. P. Abbott et al. 2017a, 2017b), have been used to constrain the binary's viewing angle (P. A. Evans et al. 2017; D. Finstad et al. 2018; K. P. Mooley et al. 2018; Y. Peng et al. 2024) and improve the standard siren H_0 measurements (C. Guidorzi et al. 2017; K. Hotokezaka et al. 2018; S. Dhawan et al. 2020; A. Palmese et al. 2024). In Figure 1, we give an example of the standard siren H_0 measurement by combining three simulated BNS observations with (orange) and without (blue) viewing angle constraints. The H_0 measurement uncertainty with viewing angle constraints is substantially smaller.

However, these constraints on viewing angle are EM model dependent, and the methods and results of different existing analyses remain to be cross-checked. Biased viewing angle constraints can lead to significant bias in H_0 (H.-Y. Chen et al. 2024). For example, the estimate of the viewing angle of

Original content from this work may be used under the terms of the Creative Commons Attribution 4.0 licence. Any further distribution of this work must maintain attribution to the author(s) and the title of the work, journal citation and DOI.

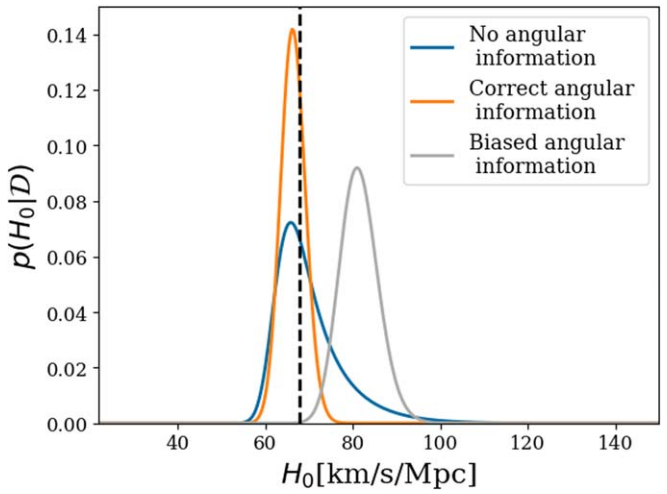

Figure 1. An example of standard siren H_0 posterior by combining three simulated 1.4–1.4$M_\odot$ BNS mergers detected by LIGO-Virgo. The blue curve assumes no extra information about the binary viewing angle. The orange curve assumes the viewing angles are constrained accurately with 1σ uncertainty of 5°, and the gray curve assumes the viewing angles are overestimated by 20° (with 1σ statistical uncertainty of 5°). The vertical dashed line indicates the H_0 value chosen for the simulations.

GW170817 varied from 22° to 50° (C. Guidorzi et al. 2017; D. Finstad et al. 2018; K. Hotokezaka et al. 2018; K. P. Mooley et al. 2018; S. Dhawan et al. 2020; J. Heinzel et al. 2021; H. Wang & D. Giannios 2021; A. Palmese et al. 2024), leading to H_0 measurements differing by more than 10% (e.g., $H_0 = 68.3^{+4.6}_{-4.5}$ km s^{-1} Mpc^{-1} by K. P. Mooley et al. 2018 and $H_0 = 75.5^{+11.6}_{-9.6}$ km s^{-1} Mpc^{-1} by C. Guidorzi et al. 2017). This is a discrepancy larger than the difference between other H_0 measurements, making it impossible to resolve the tension. In Figure 1, we give an example of the H_0 measurement assuming a 20° overestimate of the viewing angle (gray), showing the impact of the bias. The impact is expected to become more significant as the number of observations increases.

In this Letter, we develop a new method to mitigate this bias by using the viewing angle estimated from GW signals. Although the viewing angles are often poorly constrained in GWs (H.-Y. Chen et al. 2019), the measurements are well established and are expected to be unbiased (B. P. Abbott et al. 2019). Therefore, we can use the GW-inferred viewing angles from multiple observations to reveal the bias in EM observations. In the following, we first lay out our formalism. We then simulate BNSs detected by LIGO and Virgo and assume the binary viewing angles are measured inaccurately from EM observations with four different types of bias. We use these simulations to show how the biases affect the standard siren H_0 measurements. Finally, we demonstrate that our formalism successfully reduces the systematics to less than the statistical uncertainty of the H_0 measurements.

2. Mitigating the Binary Viewing Angle Bias

Although GW detectors are able to measure the angle between the total angular momentum of the binary ($\boldsymbol{J}$) and the line of sight ($\boldsymbol{N}$), the so-called inclination angle $\theta_{\rm JN}$, most EM observations only infer the binary viewing angle, ι, which is defined as $\iota \equiv \min(\theta_{\rm JN}, 180^\circ - \theta_{\rm JN})$.

For a binary with viewing angle ι_*, we assume the EM data suggests the viewing angle to be $\iota_* + b$, where b is the amount of bias. The bias is not necessarily the same for different BNS events. Suppose the biases among different events follow an unknown underlying probability density distribution—we parameterize this distribution with a vector of parameters, $\boldsymbol{\beta}$. Following this parameterization, we jointly infer H_0 and $\boldsymbol{\beta}$ using Bayesian inference and write the posterior of (H_0, $\boldsymbol{\beta}$) as

$$p(H_0, \boldsymbol{\beta}|\boldsymbol{\mathcal{D}}) = \pi(H_0, \boldsymbol{\beta})\frac{\mathcal{L}(\boldsymbol{\mathcal{D}}|H_0, \boldsymbol{\beta})}{p(\boldsymbol{\mathcal{D}})}, \tag{1}$$

where $\pi(H_0, \boldsymbol{\beta})$ stands for the prior on (H_0, $\boldsymbol{\beta}$), $\mathcal{L}(\boldsymbol{\mathcal{D}}|H_0, \boldsymbol{\beta})$ is the likelihood function, and $p(\boldsymbol{\mathcal{D}})$ is the evidence. $\boldsymbol{\mathcal{D}} \equiv (\boldsymbol{\mathcal{D}}_{\rm GW}, \boldsymbol{\mathcal{D}}_{\rm EM})$ denotes the data from GW and EM observations. When there are N BNS events, $\boldsymbol{\mathcal{D}}$ represents the collection of data $\boldsymbol{\mathcal{D}} = (\boldsymbol{\mathcal{D}}^1_{\rm GW}, \boldsymbol{\mathcal{D}}^1_{\rm EM}, \boldsymbol{\mathcal{D}}^2_{\rm GW}, \boldsymbol{\mathcal{D}}^2_{\rm EM},\ldots,\boldsymbol{\mathcal{D}}^N_{\rm GW}, \boldsymbol{\mathcal{D}}^N_{\rm EM})$. Assuming each BNS observation is independent, we can rewrite Equation (1) as

$$p(H_0, \boldsymbol{\beta}|\boldsymbol{\mathcal{D}}) \propto \pi(H_0, \boldsymbol{\beta}) \prod_{i=1}^{N} \mathcal{L}(\boldsymbol{\mathcal{D}}^i_{\rm GW}, \boldsymbol{\mathcal{D}}^i_{\rm EM}|H_0, \boldsymbol{\beta}). \tag{2}$$

If we use $\boldsymbol{\Theta}$ to denote the collection of binary physical parameters, such as luminosity distance D_L, redshift z, inclination angle $\theta_{\rm JN}$, mass, and spin, we can write the likelihood of the ith event as

$$\mathcal{L}(\boldsymbol{\mathcal{D}}^i_{\rm GW}, \boldsymbol{\mathcal{D}}^i_{\rm EM}|H_0, \boldsymbol{\beta}) = \frac{\int \mathcal{L}(\boldsymbol{\mathcal{D}}^i_{\rm GW}, \boldsymbol{\mathcal{D}}^i_{\rm EM}, \boldsymbol{\Theta}|H_0, \boldsymbol{\beta}) d\boldsymbol{\Theta}}{\int_{\boldsymbol{\mathcal{D}}_{\rm EM}>\boldsymbol{\mathcal{D}}_{\rm EM,th}}^{\boldsymbol{\mathcal{D}}_{\rm GW}>\boldsymbol{\mathcal{D}}_{\rm GW,th}} \mathcal{L}(\boldsymbol{\mathcal{D}}_{\rm GW}, \boldsymbol{\mathcal{D}}_{\rm EM}, \boldsymbol{\Theta}|H_0, \boldsymbol{\beta}) d\boldsymbol{\Theta} d\boldsymbol{\mathcal{D}}_{\rm GW} d\boldsymbol{\mathcal{D}}_{\rm EM}}, \tag{3}$$

where $\boldsymbol{\mathcal{D}}_{\rm GW,th}$ and $\boldsymbol{\mathcal{D}}_{\rm EM,th}$ denote the detection threshold of GW detectors and EM telescopes. The denominator of Equation (3) accounts for the selection effect, since not all sources are equally detectable (T. J. Loredo & D. Q. Lamb 2002; I. Mandel et al. 2019; E. Thrane & C. Talbot 2019; S. Vitale et al. 2020).

We can further separate $\boldsymbol{\Theta}$ into relevant physical parameters (D_L,z,$\Theta_{\rm JN}$) and other physical parameters $\boldsymbol{\Theta}'$ ($\boldsymbol{\Theta} \supset \{D_L, z, \Theta_{\rm JN}, \boldsymbol{\Theta}'\}$) and write the likelihood for an individual event as

$$\mathcal{L}(\boldsymbol{\mathcal{D}}^i_{\rm GW}, \boldsymbol{\mathcal{D}}^i_{\rm EM}|H_0, \boldsymbol{\beta}) \propto \int d\theta_{\rm JN} dD_{\rm L} dz d\boldsymbol{\Theta}' db \times p(\boldsymbol{\mathcal{D}}^i_{\rm GW}, \boldsymbol{\mathcal{D}}^i_{\rm EM}, \theta_{\rm JN}, D_{\rm L}, z, \boldsymbol{\Theta}', b|H_0, \boldsymbol{\beta}). \tag{4}$$

Note that in Equation (4) we explicitly write the bias b as one of the parameters that affects the data.

Since the GW and EM observations are independent, we can write the integrand of Equation (4) as (see the Appendix for step-by-step derivations)

$$p(\boldsymbol{\mathcal{D}}^i_{\rm GW}, \boldsymbol{\mathcal{D}}^i_{\rm EM}, \theta_{\rm JN}, D_{\rm L}, z, \boldsymbol{\Theta}', b|H_0, \boldsymbol{\beta}) = \mathcal{L}(\boldsymbol{\mathcal{D}}^i_{\rm GW}|\theta_{\rm JN}, D_{\rm L}, \boldsymbol{\Theta}') \times \mathcal{L}(\boldsymbol{\mathcal{D}}^i_{\rm EM}|\theta_{\rm JN}, z, \boldsymbol{\Theta}', b) \times p(\theta_{\rm JN}, D_{\rm L}, z, \boldsymbol{\Theta}', b|H_0, \boldsymbol{\beta}). \tag{5}$$

Note that the GW and EM data provide the measurements of luminosity distance D_L and redshift z, respectively, and only the EM data are affected by the viewing angle bias b.

Finally, the last term in Equation (5) can be written as

$$p(\theta_{\rm JN}, D_{\rm L}, z, \mathbf{\Theta}', b|H_0, \boldsymbol{\beta}) = \delta[D_{\rm L} - \hat{D}_{\rm L}(z, H_0)] \times p(\theta_{\rm JN}) p(z|H_0) p(\mathbf{\Theta}') p(b|\boldsymbol{\beta}). \quad (6)$$

$p(b|\boldsymbol{\beta})$ represents the probability distribution of the viewing angle bias under a given model. In this Letter, we start with a Normal distribution as our baseline model for $p(b|\boldsymbol{\beta})$. We will show later that this baseline model works well to mitigate the bias even if the bias does not follow a Normal distribution. Under this model, the probability distribution is described by two parameters, $\boldsymbol{\beta} = (\beta_1, \beta_2)$, where β_1 and β_2 represent the mean and standard deviation of the Normal distribution, respectively.

$\delta[D_{\rm L} - \hat{D}_{\rm L}(z, H_0)]$ is a Dirac δ-function originating from the dependency between luminosity distance, redshift, and H_0 when other cosmological parameters are fixed, an assumption that is valid for nearby events but can be relaxed when events at higher redshifts are included. $p(\theta_{\rm JN})$ and $p(z|H_0)$ are chosen so that the binaries are assumed to be uniformly distributed in comoving volume and have random inclination angles.

3. Application to Simulated Observations

We simulate 1000 1.4–1.4$M_\odot$ BNS detections detected by LIGO-Hanford, LIGO-Livingston, and Virgo with their fourth observing run sensitivities (`aligo_O4high.txt` and `avirgo_O4high_NEW.txt` in B. P. Abbott et al. 2020; F. Acernese et al. 2014; J. Aasi et al. 2015) in a Universe following Planck 2015 cosmology (DES & SPT Collaborations 2023; $\Omega_m = 0.306$, $\Omega_\Lambda = 0.694$, $\Omega_k = 0.0$, $H_0 = 67.8\,{\rm km\,s^{-1}\,Mpc^{-1}}$). The detections were drawn from a BNS population with isotropic orientations and are distributed uniformly in comoving volume. The GW detection threshold is set at a network signal-to-noise ratio of 12 (B. P. Abbott et al. 2020; H.-Y. Chen et al. 2021). We follow the method developed in H.-Y. Chen et al. (2019) to construct the GW likelihood function, $\mathcal{L}(\mathcal{D}^i_{\rm GW}|\theta_{\rm JN}, D_{\rm L}, \mathbf{\Theta}')$ in Equation (5). For the EM likelihood, $\mathcal{L}(\mathcal{D}^i_{\rm EM}|\theta_{\rm JN}, z, \mathbf{\Theta}', b)$, we assume that the redshift measurements from EM observations have negligible uncertainty, an appropriate assumption when compared to the uncertainty in GW distance measurements (B. P. Abbott et al. 2017a). For the viewing angle measured in EM observations, we add ϵ_* to each binary viewing angle ι_*, where ϵ_* is randomly drawn from a zero-mean Normal distribution with a standard deviation of 5°, to account for the statistical uncertainty of the measurements (P. A. Evans et al. 2017; R. Margutti et al. 2017; D. Finstad et al. 2018; K. P. Mooley et al. 2018; Y. Wu & A. MacFadyen 2018). In addition, we randomly draw a bias b_* for each binary from one of the probability distributions described below. Therefore, the likelihood of the viewing angle measured from EM observations is simulated as a one-dimensional Gaussian function with a 1σ width of 5° centering at $\tilde{\iota} = \iota_* + \epsilon_* + b_*$. To simulate the bias in viewing angle, we explore four potential probability distributions (see examples in Figure 2): (i) Normal distribution with mean γ_1 and standard deviation γ_2. This is the same type of distribution as our baseline model for $p(b|\boldsymbol{\beta})$ in Equation (6). We pick $\gamma_1 = [\pm 5°, \pm 10°, \pm 20°]$, and $\gamma_2 = 5°$. (ii) Uniform distribution, with supports $[-40°, 0°]$, $[-20°, 0°]$, $[-10°, 0°]$, $[0°, 10°]$, $[0°, 20°]$, and $[0°, 40°]$. (iii) Poisson distribution:

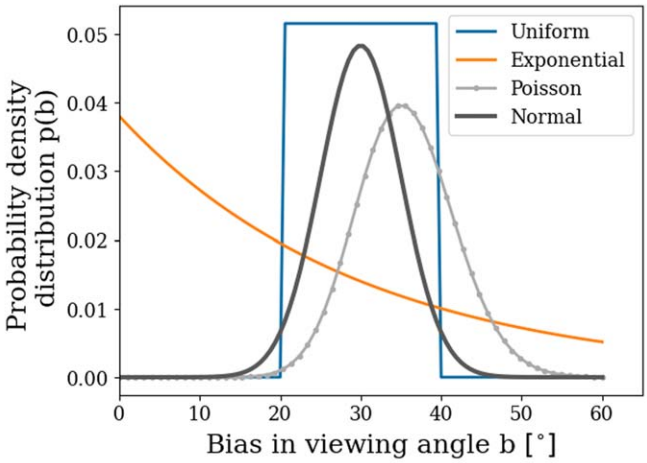

Figure 2. Probability density distribution of the bias in viewing angle we study in this Letter. The bias for each simulated BNS event is randomly drawn from these distributions.

$$p(b_*) = \begin{cases} \dfrac{\lambda^{b_*} e^{-\lambda}}{b_*!} & \text{if} \quad b_* \geqslant 0 \\ \dfrac{\lambda^{-b_*} e^{-\lambda}}{(-b_*)!} & \text{if} \quad b_* < 0 \end{cases}, \quad (7)$$

with expected rate parameter $\lambda = 10°, 20°, 30°$. (iv) Exponential distribution:

$$p(b_*) = \begin{cases} \dfrac{1}{\lambda} e^{-\frac{b_*}{\lambda}} & \text{if} \quad b_* \geqslant 0 \\ \dfrac{1}{\lambda} e^{\frac{b_*}{\lambda}} & \text{if} \quad b_* < 0 \end{cases}, \quad (8)$$

with scale parameter $\lambda = 10°, 20°, 30°$. We use uniform priors $[20, 200]\,{\rm km\,s^{-1}\,Mpc^{-1}}$, $[-90°, 90°]$, and $[2°, 92° - |\beta_1|]$ for H_0, β_1, and β_2 in Equation (1) respectively. The minimum for β_2 is chosen to avoid numerical effects in the Markov Chain Monte Carlo inference, and the maximum is set by the range of the viewing angle $[0°, 90°]$.

We randomly select 5, 10, and 20 events out of the 1000 BNS detections and use `emcee` D. Foreman-Mackey et al. (2013) to sample the posteriors in Equation (1). We repeat this process 30 times for all types of bias and report the average of posteriors in the next section.

4. Results

We start with the bias distribution that follows a Normal distribution. In the left panel of Figure 3, we present the median and symmetric 68% credible interval of the H_0 posteriors when combining 10 BNS detections for simulated bias centering at different γ_1. As shown in the figure, the H_0 measurements significantly deviate from the simulated value even with a small γ_1 when the bias is not mitigated (green). We then show the H_0 posteriors following our mitigation formalism in blue (Equation (1) marginalized over $\boldsymbol{\beta}$). We find that our formalism successfully reduces the bias in H_0 to less than their statistical uncertainties for all γ_1. In the right panel of Figure 3, we show the β_1 posteriors marginalized over H_0 and β_2 for simulated

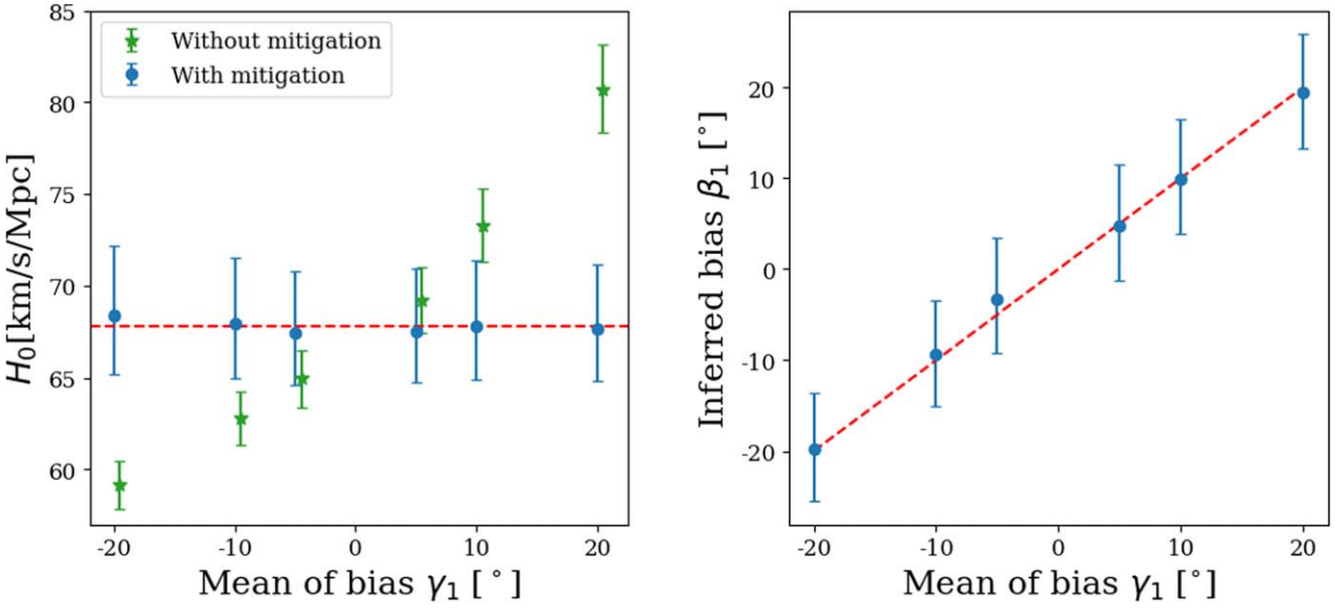

Figure 3. Measurements from 10 simulated BNS detections, averaged over 30 realizations. The horizontal axes label the mean (γ_1) of the viewing angle bias distribution. Here we assume the bias follows a Normal distribution centering at γ_1 with a standard deviation of 5°. Left: the median and symmetric 68% credible interval of the H_0 posteriors with (blue) and without (green) applying our mitigation formalism. The red dashed line marks the simulated value of H_0. Right: the median and symmetric 68% credible interval of the inferred bias (β_1) posteriors. The red dashed line represents the line of accurate measurement.

bias centering at different γ_1. We find that our formalism can reveal the simulated bias accurately.

In addition to $\sigma = 5°$ and $\gamma_2 = 5°$, we also explore larger σ and γ_2. Furthermore, we repeated the simulations for 5 and 20 BNS detections. We find similar results with H_0 and γ_1 measured accurately. In reality, the viewing angle bias distribution does not necessarily follow the parameterized model we pick. Therefore, we consider three additional types of bias distributions (Figure 2) and explore if a Normal distribution is sufficient to mitigate the bias. In Figure 4, we present the median and symmetric 68% credible interval of the H_0 posteriors with (blue) and without (green) applying our mitigation formalism for these three types of bias. Even if the bias distribution does not follow a Normal distribution, we can effectively reduce the bias in H_0 to below the measurement statistical uncertainties when modeling the bias as a Normal distribution. This is because the central limit theorem ensures the mean of the drawn biases b_* follows a Normal distribution, which can be successfully captured by our baseline model.

We also find that the inferred mean (β_1) and standard deviation (β_2) correctly estimate the mean and standard deviation of the simulated biased distribution, even if the distribution is not Normal (please see the Appendix where we present the differences).

5. Discussion

In this Letter, we present a new bright siren inference formalism that successfully mitigates the systematic uncertainty introduced by inaccurate binary viewing angle estimates. Our formalism ensures that the systematic uncertainty lies below the statistical uncertainty of the H_0 measurements when the binary viewing angle inferred from non-GW channels, such as EM observations, is biased. We show that the bias can be mitigated even if the distribution of the systematics does not precisely follow the model we assume.

The complexity of EM emission mode-lings, the differences among analyses, and the variations of observing conditions could all lead to bias in the estimate of the binary viewing angle. The sources of the bias can be difficult to disentangle, and the characteristics of the bias vary with the choice of data. It is therefore pivotal to demonstrate that our formalism effectively mitigates different types of bias distribution with the chosen baseline model, so that the formalism can be applied in wide-ranging circumstances.

In Figures 3 and 4, we present the results for 10 simulated BNS detections. We also explore the 5-detection scenario and find that 5 events are already informative enough to reveal and alleviate the bias with our formalism. In addition, we perform the 20-detection simulations to investigate if there is any remaining systematic after applying our formalism. The increased number of events reduces the statistical uncertainty of the measurements, and the systematic uncertainty stands out. We do not find any remaining bias.

Comparing the precision of the H_0 measurements with (applied our mitigation formalism) and without (no need for mitigation) using the viewing angle information, we find that the precision is comparable when the number of events is low. As the number of events increases, the bias is better inferred with our formalism, and the precision of H_0 measurements becomes better than those without using the angular information. The transition happens around 10 and 20 events when the viewing angle bias follows a Normal and Poisson distribution, respectively. We notice that the H_0 precision remains to be comparable with and without using the angular information even with 40 events for Uniform and Exponential bias distributions. This is likely due to the substantial difference between the bias distributions and our baseline model (a Normal distribution). However, if the shape of the bias distribution is better understood, more accurate models can be used to replace the Normal distribution we adopt. Even if the shape of the bias distribution is unknown, knowledge of the possible range of the bias can be used as the prior $\pi(H_0, \boldsymbol{\beta})$ in Equation (1) and improve the measurements. In addition, A nonparametric

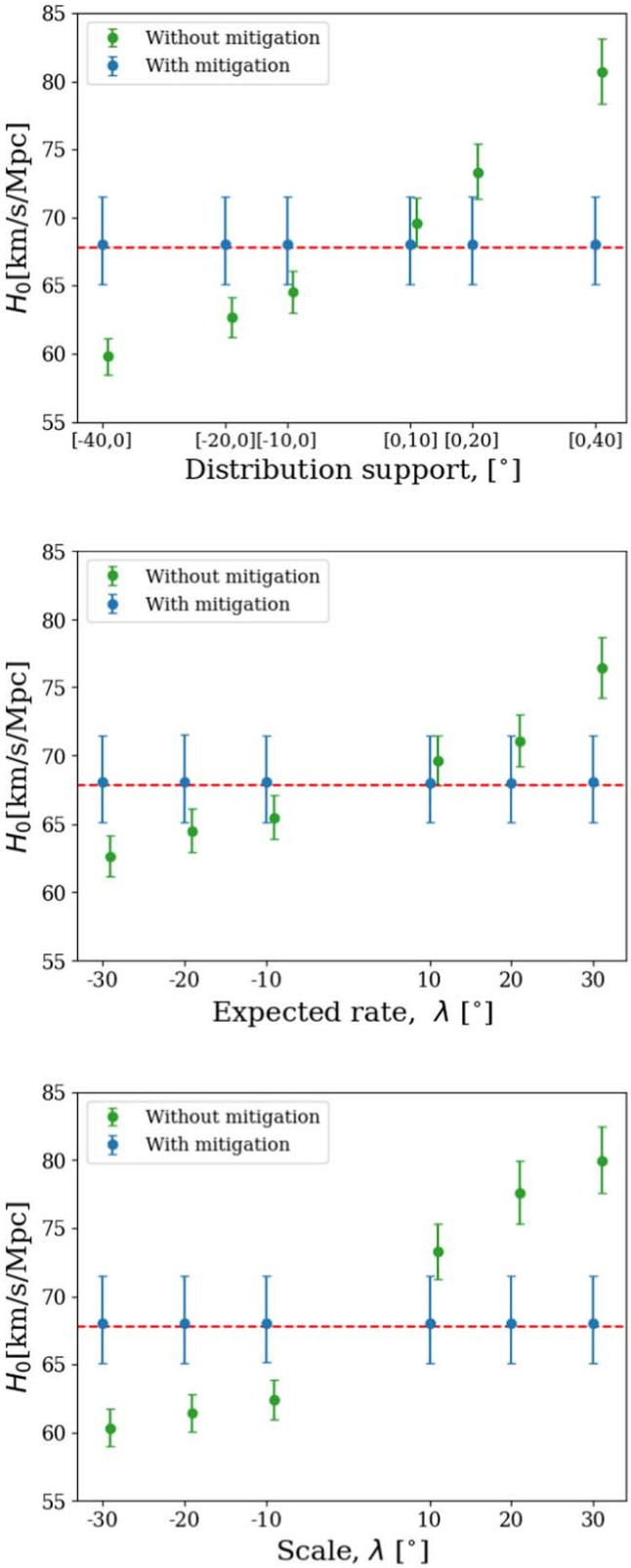

Figure 4. The median and symmetric 68% credible interval of the H_0 posteriors with (blue) and without (green) applying our mitigation formalism. We assume the viewing angle bias follows a Uniform (top), Poisson (middle), and Exponential (bottom) distribution (see texts for the choices of distribution parameters). These distributions are different from the parameterized model we pick for the bias. The results are measurements from 10 simulated BNS detections, averaged over 30 realizations.

model is another possibility to make our formalism completely model agnostic.

Acknowledgments

The authors would like to thank Sayantani Bera for the LIGO Scientific Collaboration internal review. The authors are supported by the National Science Foundation under grant PHY-2308752. The authors are grateful for the computational resources provided by the LIGO Laboratory and supported by National Science Foundation grants PHY-0757058 and PHY-0823459. This is LIGO Document Number LIGO-P2400248.

Appendix A
Likelihood

Starting from the likelihood of individual event in the main article, we apply the product rule for joint probability [$p(A, B|I) = p(A|B, I)p(B|I)$] and rewrite the integrand as

$$\begin{aligned} &p(\mathcal{D}^i_{\rm GW}, \mathcal{D}^i_{\rm EM}, \theta_{\rm JN}, D_{\rm L}, z, \mathbf{\Theta}', b|H_0, \boldsymbol{\beta}) \\ &= p(\theta_{\rm JN}, D_{\rm L}, z, \mathbf{\Theta}', b|H_0, \boldsymbol{\beta}) \\ &\quad \times p(\mathcal{D}^i_{\rm GW}, \mathcal{D}^i_{\rm EM}|\theta_{\rm JN}, D_{\rm L}, z, \mathbf{\Theta}', b, H_0, \boldsymbol{\beta}). \end{aligned} \tag{A1}$$

In the following, we repetitively apply the product rule and consider the dependencies between parameters to simplify the first line of Equation (A1):

$$\begin{aligned} &p(\theta_{\rm JN}, D_{\rm L}, z, \mathbf{\Theta}', b|H_0, \boldsymbol{\beta}) \\ &= p(D_{\rm L}|\theta_{\rm JN}, z, \mathbf{\Theta}', b, H_0, \boldsymbol{\beta}) p(\theta_{\rm JN}, z, \mathbf{\Theta}', b|H_0, \boldsymbol{\beta}) \\ &= p(D_{\rm L}|z, H_0) p(\theta_{\rm JN}|z, b, H_0, \boldsymbol{\beta}) p(z, \mathbf{\Theta}', b|H_0, \boldsymbol{\beta}) \\ &= p(D_{\rm L}|z, H_0) p(\theta_{\rm JN}) p(\mathbf{\Theta}') p(z|H_0) p(b|\boldsymbol{\beta}) \\ &= \delta[D_{\rm L} - \hat{D}_{\rm L}(z, H_0)] p(\theta_{\rm JN}) p(\mathbf{\Theta}') p(z|H_0) p(b|\boldsymbol{\beta}). \end{aligned} \tag{A2}$$

The second equality originates from the fact that the intrinsic distribution of source luminosity distance is independent of the binary inclination angle $\theta_{\rm JN}$, the viewing angle bias b, and the bias parameters $\boldsymbol{\beta}$. Similarly, the third equality indicates that the intrinsic distribution of binary inclination angle $\theta_{\rm JN}$ is independent of other parameters. The redshift z distribution only depends on H_0 when other cosmological parameters are fixed. The viewing angle bias b only depends on the bias distribution parameters $\boldsymbol{\beta}$. Finally, the dependency between D_L, z and H_0 leads to the last line.

Since GW and EM observations are independent, we separate the second line of Equation (A1) into

$$\begin{aligned} &p(\mathcal{D}^i_{\rm GW}, \mathcal{D}^i_{\rm EM}|, \theta_{\rm JN}, D_{\rm L}, z, \mathbf{\Theta}', b, H_0, \boldsymbol{\beta}) \\ &= \mathcal{L}(\mathcal{D}^i_{\rm GW}|\theta_{\rm JN}, D_{\rm L}, z, \mathbf{\Theta}', b, H_0, \boldsymbol{\beta}) \\ &\quad \times \mathcal{L}(\mathcal{D}^i_{\rm EM}|\theta_{\rm JN}, D_{\rm L}, z, \mathbf{\Theta}', b, H_0, \boldsymbol{\beta}). \end{aligned} \tag{A3}$$

We can further simplify this expression by accounting for the dependencies of parameters. The GW data are independent of the viewing angle biases b and their distribution parameters $\boldsymbol{\beta}$. Furthermore, GW data do not directly depend on z or H_0.

Therefore,

$$\mathcal{L}(\boldsymbol{\mathcal{D}}^i_{\rm GW}|\theta_{\rm JN}, D_{\rm L}, \boldsymbol{\Theta}', b, \boldsymbol{\beta}) = \mathcal{L}(\boldsymbol{\mathcal{D}}^i_{\rm GW}|\theta_{\rm JN}, D_{\rm L}, \boldsymbol{\Theta}'). \quad \text{(A4)}$$

On the other hand, EM observations provide the measurements of redshift z, and the inclination angle estimate is biased by the bias b under our following assumption:

$$\mathcal{L}(\boldsymbol{\mathcal{D}}^i_{\rm EM}|\theta_{\rm JN}, D_{\rm L}, z, \boldsymbol{\Theta}', b) = \mathcal{L}(\boldsymbol{\mathcal{D}}^i_{\rm EM}|\theta_{\rm JN}, z, \boldsymbol{\Theta}', b). \quad \text{(A5)}$$

We note that the EM likelihood Equation (A5) is symmetric around $\theta_{\rm JN} = 90°$, since the EM observations only measure the viewing angle.

Appendix B
Inference of the Viewing Angle Bias

We compute the difference between the median of the inferred mean (i.e., median of the β_1 posterior) and the mean of the simulated bias. We repeat the computation for 30 realizations and present the median and symmetric 68% credible interval of the difference (Figures 5 and 6). Similarly, we compute the difference between the median of the inferred standard deviation (i.e., median of the β_2 posterior) and the standard deviation of the simulated bias. We then present the median and symmetric 68% credible interval of the difference over 30 realizations (Figures 7 and 8). The results are shown for all three types of non-Normally distributed bias in the manuscript. We show the results when combining 10 and 20 events. We find that the means of the bias distribution can be

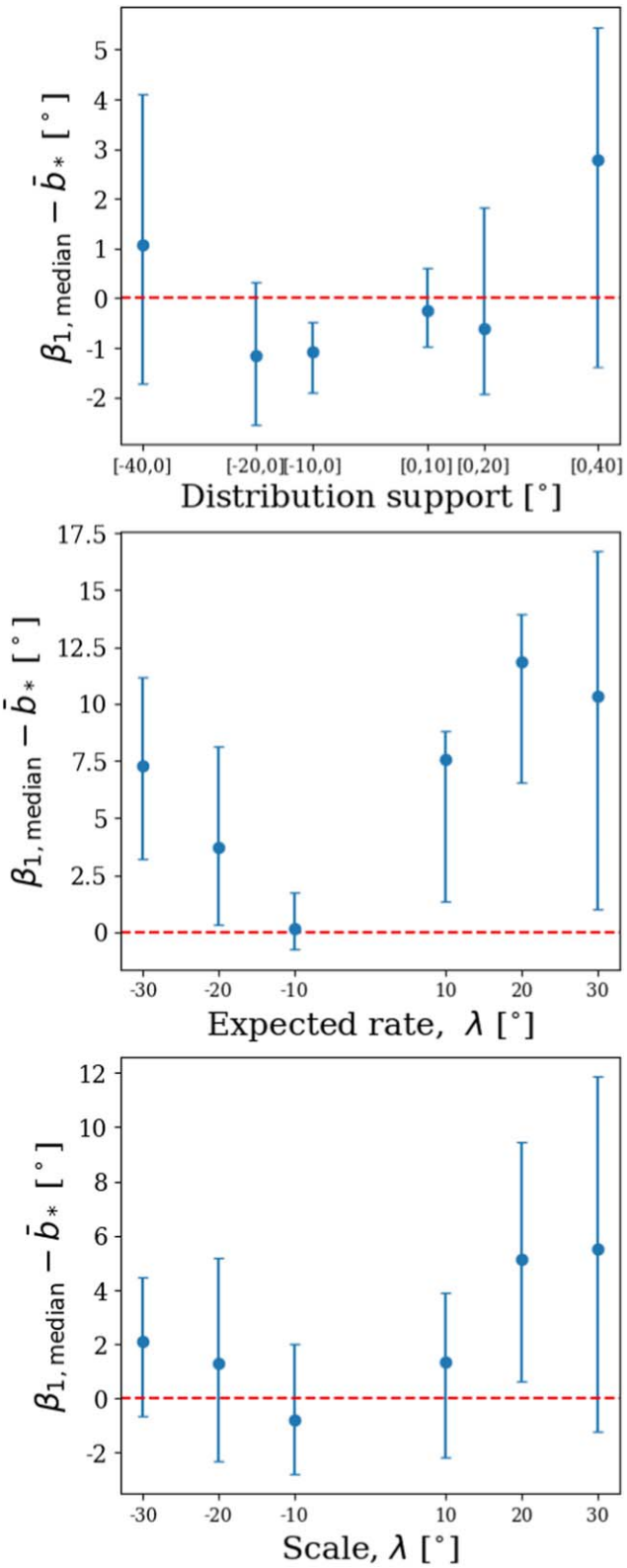

Figure 5. The difference between the median of the inferred mean (i.e., median of the β_1 posterior) and the mean of the simulated bias when combining 10 simulated BNS events. The data point and error bar show the median and symmetric 68% credible interval of the difference for 30 realizations. The results are for the viewing angle bias following a Uniform (top), Poisson (middle), and Exponential (bottom) distribution.

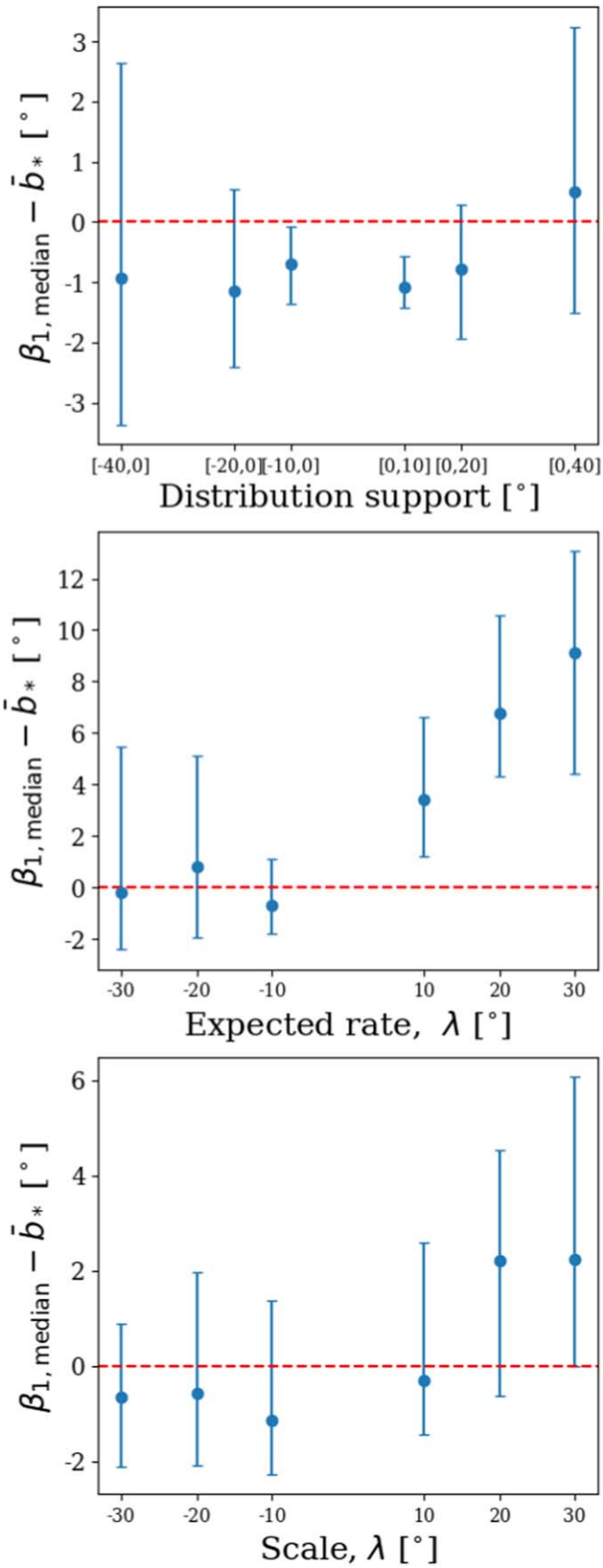

Figure 6. Same as Figure 5 but combining 20 simulated BNS events.

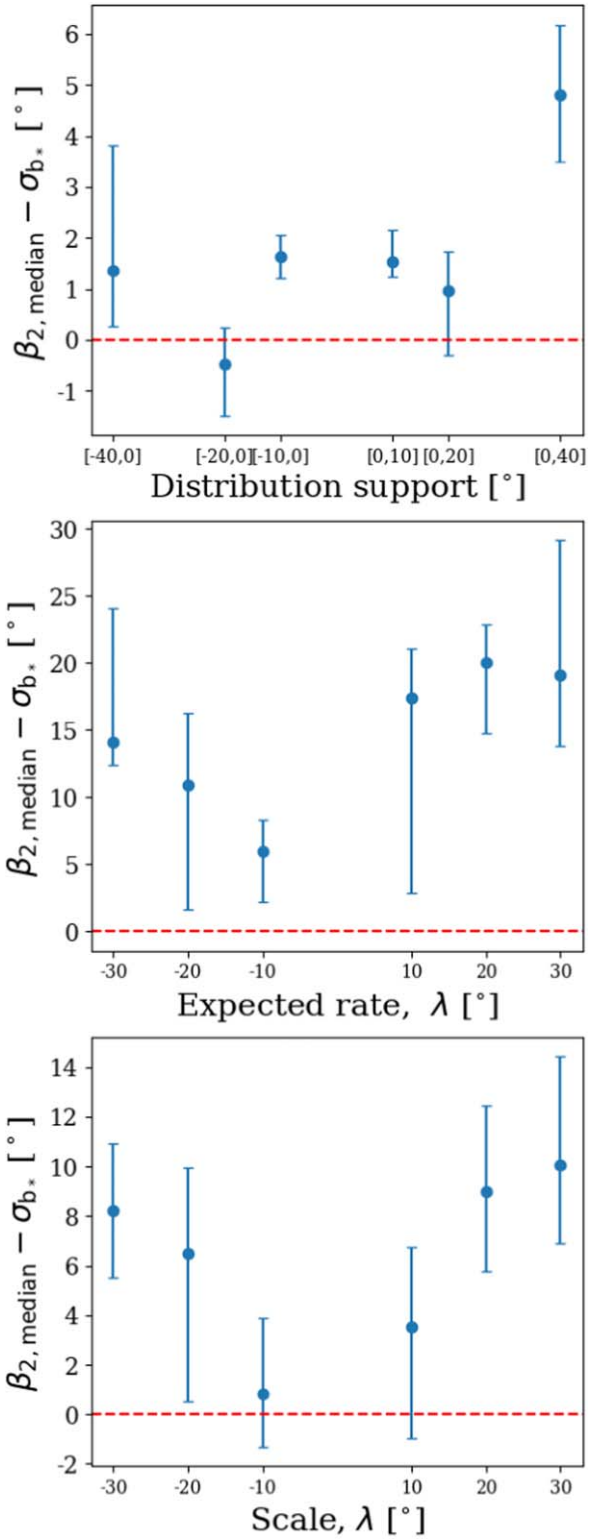

Figure 7. The difference between the median of the inferred standard deviation (i.e., median of the β_2 posterior) and the standard deviation of the simulated bias when combining 10 simulated BNS events. The data point and error bar show the median and symmetric 68% credible interval of the difference for 30 realizations. The results are for the viewing angle bias following a Uniform (top), Poisson (middle), and Exponential (bottom) distribution.

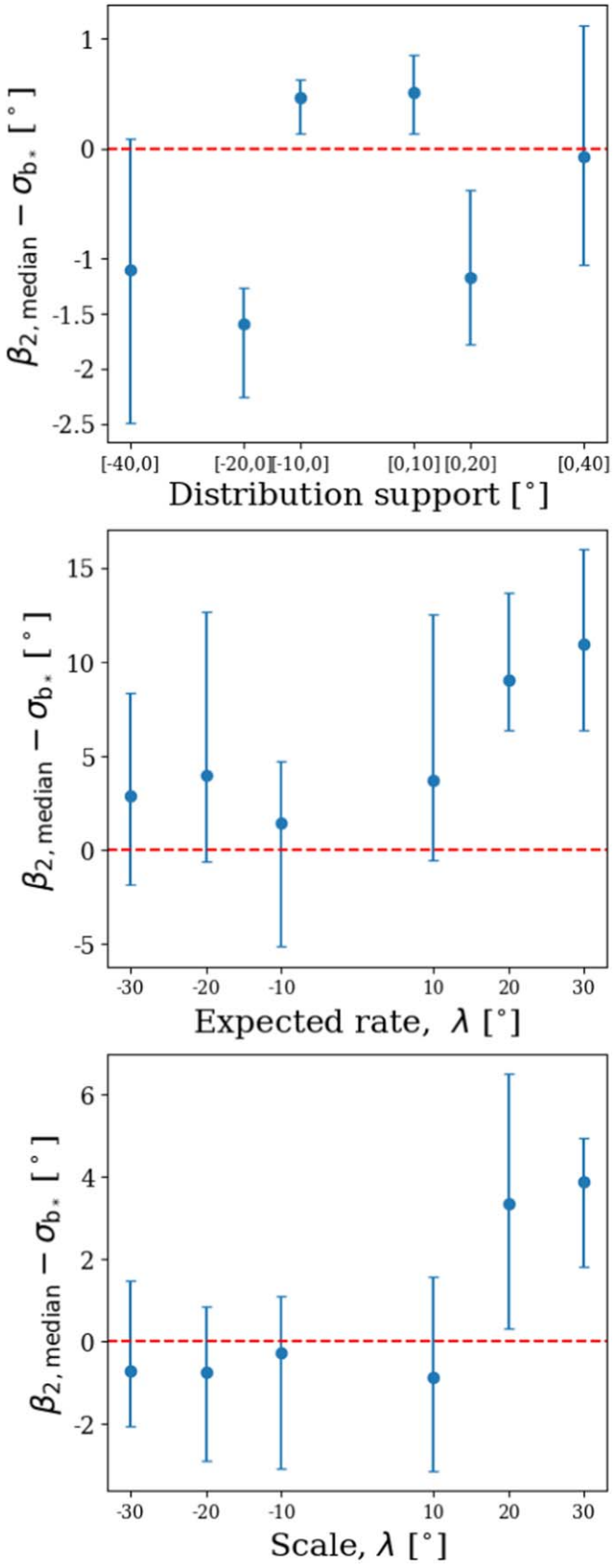

Figure 8. Same as Figure 7 but combining 20 simulated BNS events.

inferred fairly well with $\gtrsim$10 events, and the standard deviations can be inferred with $\gtrsim$20 events.

ORCID iDs

Alberto Salvarese https://orcid.org/0000-0001-9653-1778
Hsin-Yu Chen https://orcid.org/0000-0001-5403-3762

References

Aasi, J., Abadie, J., Abbott, B. P., et al. 2015, CQGra, 32, 074001
Abbott, B. P., Abbott, R., Abbott, T. D., et al. 2017a, PhRvL, 119, 161101
Abbott, B. P., Abbott, R., Abbott, T. D., et al. 2017b, ApJL, 848, L12
Abbott, B. P., Abbott, R., Abbott, T. D., et al. 2019, PhRvX, 9, 011001
Abbott, B. P., Abbott, R., Abbott, T. D., et al. 2020, LRR, 23, 23
Acernese, F., Agathos, M., Agatsuma, K., et al. 2014, CQGra, 32, 024001
Aghanim, N., Akrami, Y., Ashdown, M., et al. 2020, A&A, 641, A6
Alam, S., Ata, M., Bailey, S., et al. 2017, MNRAS, 470, 2617
Chen, H.-Y., Fishbach, M., & Holz, D. E. 2018, Natur, 562, 545
Chen, H.-Y., Holz, D. E., Miller, J., et al. 2021, CQGra, 38, 055010
Chen, H.-Y., Talbot, C., & Chase, E. A. 2024, PhRvL, 132, 191003
Chen, H.-Y., Vitale, S., & Narayan, R. 2019, PhRvX, 9, 031028
DES & SPT Collaborations 2023, PhRvD, 107, 023531
Dhawan, S., Bulla, M., Goobar, A., Sagués Carracedo, A., & Setzer, C. N. 2020, ApJ, 888, 67
Di Valentino, E., Mena, O., Pan, S., et al. 2021, CQGra, 38, 153001
Evans, P. A., Cenko, S. B., Kennea, J. A., et al. 2017, Sci, 358, 1565
Feeney, S. M., Peiris, H. V., Williamson, A. R., et al. 2019, PhRvL, 122, 061105
Finstad, D., De, S., Brown, D. A., Berger, E., & Biwer, C. M. 2018, ApJL, 860, L2
Foreman-Mackey, D., Hogg, D. W., Lang, D., & Goodman, J. 2013, PASP, 125, 306
Guidorzi, C., Margutti, R., Brout, D., et al. 2017, ApJL, 851, L36
Heinzel, J., Coughlin, M. W., Dietrich, T., et al. 2021, MNRAS, 502, 3057
Holz, D. E., & Hughes, S. A. 2005, ApJ, 629, 15
Hotokezaka, K., Nakar, E., Gottlieb, O., et al. 2018, NatAs, 3, 940
Kamionkowski, M., & Riess, A. G. 2023, ARNPS, 73, 153
Loredo, T. J., & Lamb, D. Q. 2002, PhRvD, 65, 063002
Mandel, I., Farr, W. M., & Gair, J. R. 2019, MNRAS, 486, 1086
Margutti, R., Berger, E., Fong, W., et al. 2017, ApJL, 848, L20
Mooley, K. P., Deller, A. T., Gottlieb, O., et al. 2018, Natur, 561, 355
Nissanke, S., Holz, D. E., Dalal, N., et al. 2013, arXiv:1307.2638
Palmese, A., Kaur, R., Hajela, A., et al. 2024, PhyRvD, 109, 063508
Peng, Y., Ristić, M., Kedia, A., et al. 2024, PhRvR, 6, 033078
Riess, A. G., Macri, L. M., Hoffmann, S. L., et al. 2016, ApJ, 826, 56
Riess, A. G., Yuan, W., Macri, L. M., et al. 2022, ApJL, 934, L7
Ross, A. J., Samushia, L., Howlett, C., et al. 2015, MNRAS, 449, 835
Schutz, B. F. 1986, Natur, 323, 310
Thrane, E., & Talbot, C. 2019, PASA, 36, e010
Verde, L., Treu, T., & Riess, A. G. 2019, NatAs, 3, 891
Vitale, S., Gerosa, D., Farr, W. M., & Taylor, S. R. 2020, Handbook of Gravitational Wave Astronomy (Singapore: Springer), 1
Wang, H., & Giannios, D. 2021, ApJ, 908, 200
Wu, Y., & MacFadyen, A. 2018, ApJ, 869, 55